Scientific Research Publishing

World Journal of Condensed Matter Physics, 2024, 14, 10-20
https://www.scirp.org/journal/wjcmp
ISSN Online: 2160-6927
ISSN Print: 2160-6919

Investigation of Acoustomagnetoelectric Effect in Bandgap Graphene by the Boltzmann Transport Equation

Raymond Edziah[1*], Samuel S. Bentsiefi[1], Kwadwo Dompreh[1], Anthony Twum[1], Emmanuel Kofi Amewode[1], Patrick Mensah-Amoah[1], Ebenezer T. Tatchie[1], Cynthia Jebuni-Adanu[2], Samuel Y. Mensah[1]

[1]Department of Physics, University of Cape Coast, Cape Coast, Ghana
[2]Department of Physics Education, University of Education, Winneba, Ghana
Email: *redziah@ucc.edu.gh

How to cite this paper: Edziah, R., Bentsiefi, S.S., Dompreh, K., Twum, A., Amewode, E.K., Mensah-Amoah, P., Tatchie, E.T., Jebuni-Adanu, C. and Mensah, S.Y. (2024) Investigation of Acoustomagnetoelectric Effect in Bandgap Graphene by the Boltzmann Transport Equation. *World Journal of Condensed Matter Physics*, **14**, 10-20.
https://doi.org/10.4236/wjcmp.2024.141002

Received: November 23, 2023
Accepted: February 2, 2024
Published: February 5, 2024

Abstract

We study the acoustomagnetoelectric (AME) effect in two-dimensional graphene with an energy bandgap using the semiclassical Boltzmann transport equation within the hypersound regime, $k_q l \gg 1$ (where k_q represents the acoustic wavenumber and l is the mean free path of the electron). The Boltzmann transport equation and other relevant equations were solved analytically to obtain an expression for the AME current density, consisting of longitudinal and Hall components. Our numerical results indicate that both components of the AME current densities display oscillatory behaviour. Furthermore, geometric resonances and Weiss oscillations were each defined using the relationship between the current density and Surface Acoustic Wave (SAW) frequency and the inverse of the applied magnetic field, respectively. Our results show that the AME current density of bandgap graphene, which can be controlled to suit a particular electronic device application, is smaller than that of (gapless) graphene and is therefore, more suited for nanophotonic device applications.

Keywords

Boltzmann Transport Equation, Acoustomagnetoelctric Effect, Surface Acoustic Wave, Gapless Graphene, Weiss Oscillations

1. Introduction

Ever since the discovery of (gapless) graphene, a two-dimensional (2D) material

having an intrinsic strength of 42 $N \cdot m^{-1}$, electron mobility of more than 42,000 $cm^2 \cdot V^{-1} \cdot s^{-1}$, thermal conductivity of 5000 $W \cdot m^{-1} \cdot K^{-1}$ and Young's modulus of 1000 GPa [1] [2], research into two-dimensional (2D) systems has been on the ascendancy. Despite these intriguing properties, graphene has not been fully utilized for device applications due to several factors, prominent of which is the absence of a bandgap in its electronic structure. As a result, several methods have been proposed to overcome the challenge imposed on this novel material by its lack of bandgap. Theoretically, it has been suggested that an energy gap can be induced into the structure of a bilayer of gapless graphene whenever a high electric field is applied vertically across it [3] [4]. Practically, it is feasible to introduce an energy gap into a gapless graphene by placing it on a substrate as demonstrated in the case of graphene on a boron nitride (BN) substrate [5]. The BN substrate is made up of layers of these two crystals that alternate on a regular basis in a specific direction and as such modulates the gap produced in the graphene. Therefore, unlike its gapless counterpart, bandgap graphene is more suitable for nanophotonic device applications. Some of the key advantages of bandgap graphene include its tunability, high carrier mobility, broadband absorption, and the possibility of its integration with silicon photonics. These properties enable applications such as high-speed photodetectors, optical modulators, sensors, flexible electronics, and integrated photonics. Bandgap graphene's unique combination of characteristics holds promise for advancing technologies in communication, sensing, and optical signal processing.

Surface acoustic waves (SAWs) are modes of elastic energy propagating along the surface of an elastic medium (such as a piezoelectric material) and result from coupling between longitudinal and shear waves. Surface acoustic waves have been used to study acoustic charge transport (ACT) in low-dimensional systems such as gapless graphene. An acoustoelectric effect occurs whenever there is a strong interaction between the piezoelectric fields associated with a SAW propagating on a piezoelectric substrate and a charge carrier system [6]. Consequently, acoustoelectric (AE) currents are generated whenever the piezoelectric potentials trap and transport charge at the speed of sound [7] [8]. Since its discovery in the 1950s, the AE effect has been extensively studied in both metals and bulk and low-dimensional semiconductors. The AE effect has been investigated theoretically in carbon nanotubes (CNTs) and superlattices (SLs) [9], as well as experimentally in vanadium oxide films [10]. Other studies have examined the valley AE effect in 2D materials such as a transition metal dichalcogenide monolayer coupled to a piezoelectric substrate [11].

The Boltzmann transport equation (BTE) has been used in conjunction with SAWs to theoretically study AE current as either a classical coherent force or a noncoherent quasi-monochromatic phonon flux [6] [12] [13] [14]. This approach to electron description is valid for high temperatures. Here, SAWs were used to transport and manipulate charge carriers in a crystal. The SAW propagates by dragging conduction electrons, and the electric current has been shown to possess the shape of Shubnikov–de Haas oscillations [14] [15]. When the

magnetic field is inverted, as in the case of the acoustomagnetoelectric (AME) effect, the AE current also displays periodic Weiss oscillations due to the commensurability between the spatial period in the crystal, the cyclotron orbit size, and resonances at the SAW frequency. Other magneto-oscillations such as geometric resonances (GRs) have been reported both theoretically and experimentally.

Theoretical studies have examined quantum Hall effects, conductivity and higher current density harmonics in both gapless and bandgap graphene [16] [17]. Other studies also focused on AME effect in graphene nanoribbons [6] [18]. However, to the best of our knowledge, no study has been reported on the electronic properties of graphene having an energy gap due to the AME effect. This study will therefore, investigate the AME effect in a graphene with an energy bandgap by employing the BTE within the hypersound regime, $k_q l \gg 1$ (where k_q represents the acoustic wavenumber and l is the mean free path of the electron), a condition in which the hypersound wavelength is far smaller than the electron mean free path.

2. Theory

The AME effect in the bandgap graphene is studied using the semiclassical BTE by deriving an expression for the AME current. The study focused only on the situation where an electron is reflected in two dimensions off of the surface of the graphene crystal. The piezoelectric potential mechanism serves as the foundation for the electron-acoustic phonon interaction. The dispersion relation of the bandgap graphene is expressed in the form [17]:

$$\varepsilon_p = \left\{ \Delta^2 + \gamma^2 \left[1 + 4\cos\left(\frac{p_y a}{\sqrt{3}} \right) \left\{ \cos\left(\frac{p_x a}{\sqrt{3}} \right) + \cos\left(\frac{p_y a}{\sqrt{3}} \right) \right\} \right] \right\}^{\frac{1}{2}} \tag{1}$$

where $\gamma \approx 2.7\ \text{eV}$ is the electron transition energy between neighbouring sites of the graphene lattice, Δ is the bandgap half-width, p is the quasimomentum of the electron, $a = \frac{3b}{2\hbar}$, $b = 0.142\ \text{nm}$ is the distance between neighbouring carbon atoms in graphene and $\hbar$ is the reduced Planck's constant.

Consider a SAW which is typically produced by patterned metallic gates known as Interdigital Transducers (IDTs) on top of a piezoelectric substrate as schematically shown in **Figure 1** [16].

Along the wave's direction of travel, the SAW produced by the IDT creates an electric field. When the rf signal is applied to the IDTs, the spacing of the pitch could be used to determine the SAW wavelength so that its product with the rf frequency equals the sound velocity in the crystal. Under this condition, the piezoelectric field modulates the electron density and charge carrier velocity. As a result, the AE current becomes the constant component of the electric current density. In the presence of an external magnetic field, the stationary second-order adjustment to the distribution function with respect to the SAW's piezoelectric field can be used to calculate the acoustoelectric current. In this case, the BTE has the form:

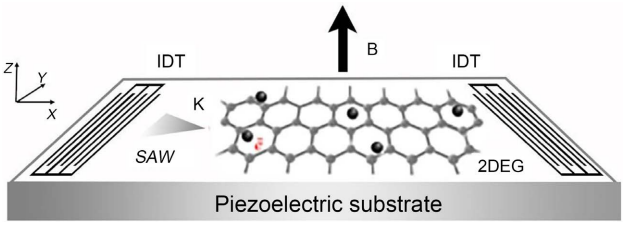

Figure 1. A two-dimensional electron gas (2DEG) with parabolic or linear (graphene) spectrum located on a piezoelectric substrate and exposed to a surface acoustic wave (SAW) with the wave vector k and an external permanent magnetic field B (adapted from Ref. [16]). The SAW is created by the interdigital transducers (IDTs).

$$\left[\frac{\partial}{\partial t}+v\frac{\partial}{\partial r}+e\left\{E\left(r,t\right)+E^{i}\left(r,t\right)+\left[v\times B\right]\right\}\frac{\partial}{\partial p}\right]f=-\upsilon\left\{f-\left\langle f\right\rangle\right\} \tag{2}$$

where $\left\langle f\right\rangle$ is the quasi-equilibrium distribution function, $f\left(r,t\right)$ is the distribution function, v is the velocity of electron and $\upsilon=\frac{1}{\tau}$ with τ being the effective relaxation time, which is assumed to be constant. Here, $\tau=\frac{\mu_e p}{ev}$ with μ_e representing the charge mobility. The total electric field is given as $\tilde{E}\left(r,t\right)=E^{i}\left(r,t\right)+E\left(r,t\right)$, where $E^{i}\left(r,t\right)$ is the induced electric field and B is the applied magnetic field.

The AE current is determined by expanding the distribution function and electron density up to the second order with respect to the total electric field. Specifically, $f\left(r,t\right)=f_0+f_1\left(r,t\right)+f_2\left(r,t\right)+O\left(f_3\right)$ where f_0 is the equilibrium distribution function. The first-order correction is given as

$$f_1\left(r,t\right)=\frac{1}{2}\left[f_1\exp\left(ik_q\cdot r-i\omega_q t\right)+f_1^{*}\exp\left(-ik_q\cdot r+i\omega_q t\right)\right],$$

where $\omega_q=v_s\left|k_q\right|$, v_s representing the velocity of sound, f_1^{*} is the complex conjugate of f_1 and k_q and ω_q are the wavenumber and wave frequency, respectively.

Assume the SAW travels along the *x*-axis and an external magnetic field is applied perpendicular to the direction of travel of the wave. Under this condition, the time-independent acoustoelectric current can be derived from the stationary second-order correction to the distribution function f_2 of the electron with respect to the SAW field as:

$$j^{AME}=e\int\frac{\mathrm{d}p}{\left(2\pi\hbar\right)^2}vf_2 \tag{3}$$

such that

$$\begin{aligned}j_n^{AME}=&-\frac{e^2}{2\omega_c}\int\int_0^{\infty}\mathrm{d}\psi\frac{\mathrm{d}p}{\left(2\pi\hbar\right)^2}v_n\left(\phi\right)\mathrm{e}^{-\frac{\psi}{\omega_c\tau_1}}\left(1-\frac{\psi}{\omega_c\tau_1}\right)\\&\times Re\left\{E_0 v\cos\left(\phi+\psi\right)\frac{\partial f_1\left(p,\phi+\psi\right)}{\partial\varepsilon_p}\right\};n=x,y\end{aligned} \tag{4}$$

where $v_n(\phi)=v(\cos\phi,\sin\phi)$, $\tau_1=\frac{\tau}{2}$, E_o is the amplitude of the piezoelectric field, e is the electron charge, $v=\frac{\partial\varepsilon_p}{\partial p}$ and f_1 is the solution of the BTE (Equation (2)) and can be expressed as:

$$f_1=\tau e^{i\beta_g\sin\phi}\left(-\frac{\partial f_o}{\partial\varepsilon_p}\right)\sum_{u=-\infty}^{\infty}\left(\frac{eE_0v}{\beta_g}u+\frac{n_1}{\tau}\frac{\partial\mu}{\partial n}\right)\frac{J_u(\beta_g)e^{iu\phi}}{1-i\left[\omega_q-u\omega_c\right]\tau} \tag{5}$$

where $\omega_c=\frac{eBv}{p}$ is the semiclassical cyclotron frequency and $J_u(\beta_g)$ is the Bessel function of the u^{th} order with argument $\beta_g=\frac{k_qv}{\omega_c}$. The derivative of the chemical potential $\mu(r,t)$ with respect to the charge density is expressed as:

$$\frac{\partial\mu}{\partial n}=\frac{\pi\hbar^2}{m} \tag{6}$$

The first-order correction to the charge density n_1 is derived from the solutions of the induced E-field and the continuity equation as:

$$n_1=\frac{\sigma_{xx}E_o}{e(v_s-R_x)g(\omega_q,k_q)} \tag{7}$$

where the *xx*-component of the conductivity tensor

$$\sigma_{xx}=\frac{p^2}{\pi\hbar^2}\frac{\sigma_g}{\beta_g^2}\sum_{u=-\infty}^{\infty}\frac{u^2J_u^2(\beta_g)}{1-i(\omega_q-\omega_cu)\tau} \tag{8}$$

with $\sigma_g=\frac{e^2nv\tau}{p}$ being the Drude conductivity. The *x*-component of the diffusion vector

$$R_x=\frac{2\omega_c}{k_q}\sum_{u=-\infty}^{\infty}\frac{uJ_u^2(\beta_g)}{1-i(\omega_q-\omega_cu)\tau} \tag{9}$$

and

$$g(\omega_q,k_q)=1+i\frac{1}{\varepsilon_o(\varepsilon_d+1)}\frac{\sigma_{xx}}{v_s-R_x} \tag{10}$$

is the dielectric function, ε_d is the substrate's dielectric constant and ε_0 is the permittivity of free space. The absorption of the SAW's piezoelectric field by the mobile electron in the 2D system is described by Equation (10).

Substituting Equation (5)-Equation (7) into Equation (4), the AME current density is obtained as:

$$\begin{aligned}\begin{pmatrix}j_x^{AME}\\ j_y^{AME}\end{pmatrix}=&Re\frac{e^2E_o}{2\omega_c(2\pi\hbar)^2}\int_0^{\infty}d\varepsilon_p\frac{e^{i\beta_g\sin(\phi+\psi)}}{i\omega_c}\left(-\frac{\partial f_o}{\partial\varepsilon_p}\right)\\&\times\sum_{r=-\infty}^{\infty}\left(\frac{eE_ov}{\beta_g}u+\frac{n_1}{\tau}\frac{\partial\mu}{\partial n}\right)\frac{J_u(\beta_g)e^{-iu(\phi+\psi)}}{(u-\alpha_g)}\\&\times\int_0^{\infty}d\psi\,e^{-\frac{\psi}{\omega_c\tau_1}}\left(1-\frac{\psi}{\omega_c\tau_1}\right)\int_0^{2\pi}d\phi\cos(\phi+\psi)\begin{Bmatrix}\cos\phi\\ \sin\phi\end{Bmatrix}\end{aligned} \tag{11}$$

where j_x^{AME} and j_y^{AME} are the longitudinal and Hall AME current densities, respectively and $\alpha_g = \dfrac{\omega_q + \dfrac{i}{\tau}}{\omega_c}$. Simplifying Equation (10) yields

$$\begin{pmatrix} j_x^{AME} \\ j_y^{AME} \end{pmatrix} = \frac{\tau\omega_c p^2}{16env\pi\hbar^2}\left|\sigma_g E_o\right|^2 \left(\frac{\dfrac{2}{\beta_g}}{1+\omega_c^2\tau^2}\right)^2 \times Re\sum_{u=-\infty}^{\infty}\frac{J_u\left(\beta_g\right)}{1-i\left(\omega_q-\omega_c u\right)\tau}$$
$$\times\left(u+\frac{k_q b_g}{2\omega_c\tau}\frac{\sigma_{xx}}{\varepsilon_o\left(v_s-R_x\right)g\left(\omega_q,k_q\right)}\right) \tag{12}$$
$$\times\begin{Bmatrix} -i\overline{\gamma}^2\left(u+1\right)J_{u+1}\left(\beta_g\right)+i\overline{\gamma}^{*2}\left(u-1\right)J_{u-1}\left(\beta_g\right) \\ \overline{\gamma}^2\left(u+1\right)J_{u+1}\left(\beta_g\right)+\overline{\gamma}^{*2}\left(u-1\right)J_{u-1}\left(\beta_g\right) \end{Bmatrix}$$

where

$$b_g = \frac{2\pi\hbar^2\varepsilon_o v}{e^2 p} \quad \text{and} \quad \overline{\gamma} = 1 + i\omega_c\tau$$

3. Results and Discussion

The AME effect in a degenerate 2DEG has been studied using the semiclassical BTE together with other relevant equations, resulting in the derivation of an expression for the AME current. The argument β_g of the Bessel functions in Equations (9), (11) and (12) is of particular relevance and can be expressed as $\beta_g = \dfrac{k_q v}{\omega_c} = \dfrac{\omega_q v}{v_s\omega_c}$, which is similar to the well-known expression for geometric resonances (GRs) in terms of the ratio of frequencies and determines the strength of the resonances. In contrast, β_g in our study describes the ratio of space scales as $\beta_g = k_q c_r = \dfrac{2\pi c_r}{\lambda_q}$, where c_r is the cyclotron radius, which is similar to Weiss oscillations [16].

To further provide a practical meaning to our analytical results, the AME current is examined in this section as two distinct components: the longitudinal (*x*-component) AME current drag and the Hall (*y*-component) AME current drag. Our numerical analysis took into account the following variables which can be realized experimentally [16] [19]: $n = 5\times10^{12}\ \text{cm}^{-2}$, $h = 4.1356\times10^{-15}\ \text{eV}\cdot\text{s}^{-1}$, $\varepsilon_d = 50$, $E_0 = 10\ \text{kV/m}$, $v_s = 3.5\times10^3\ \text{m/s}$, $\Delta = 2.7\ \text{eV}$, $\mu_e = 10^4\ \text{cm}^2/\text{V}\cdot\text{s}$, $m = 0.44m_0$ where m_0 is the mass of free electron.

Figure 2 shows a plot of the longitudinal (*x*-component) and Hall (*y*-component) of AME current densities, $j_{x,y}^{AME}$ as functions of SAW frequency, ω_q for various values of the magnetic field, *B*.

It is observed that as ω_q increases, j_x^{AME} increases from the negative region to a threshold value within the neighborhood of $j_x^{AME} = 0$ and oscillates. Similar observations are made for the dependence of the Hall AME current density on SAW frequency for the same values of *B*. This is because the charge carriers

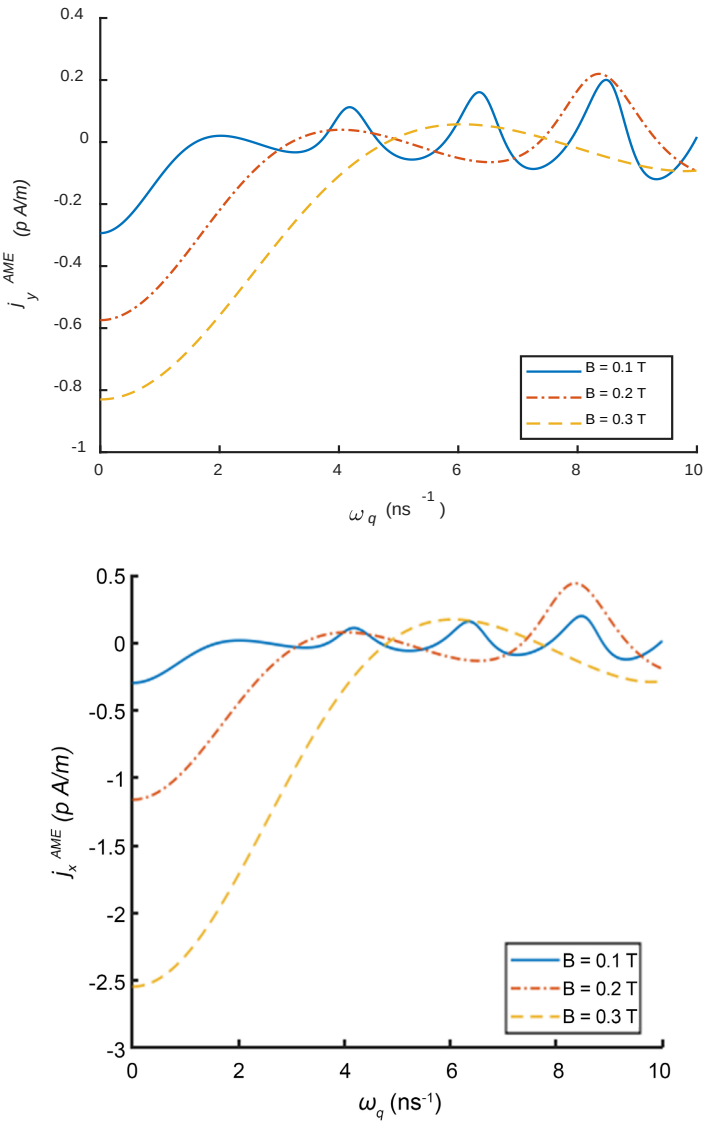

Figure 2. Dependence of AME current density $\begin{pmatrix} j_x^{AME} \\ j_y^{AME} \end{pmatrix}$ on the SAW frequency ω_q for selected values of the applied magnetic field *B*.

tend to travel in the direction of the applied B-field in the process of absorption of SAW within the crystal. The oscillations observed in our study are similar to those seen in [16], in which the AME current density decreases from a positive region and decays monotonically to zero. The difference in the behaviours could be attributed to the presence of a bandgap, which is fundamentally required for electronic device applications. The oscillations in both components of the AME current are distinct with each maximum roughly coinciding with the geometric resonance $\omega_q = r\omega_c$, where *r* is an integer. As expected, with relatively low SAW frequencies, geometric resonances become apparent at magnetic fields less than 1 T, and the cyclotron frequency increases with the applied magnetic field. At higher fields (*i.e.*, $\omega_q\tau > 1$), the monotone functions show no geometric reso-

nance-related oscillations. Additionally, when $\omega_c \tau \gg 1$, the absorption exhibits resonant behavior with the field, a behaviour which is typically observed in crossed electric and magnetic fields.

Figure 3 represents the dependence of longitudinal and Hall AME current densities $j_{x,y}^{AME}$ on the inverse magnetic field, B^{-1} for different values of the SAW frequency ω_q.

Figure 3 shows that j_x^{AME} increases to some threshold value and decreases asymptotically with small oscillations afterwards. As B^{-1} increases, j_y^{AME} increases asymptotically from the negative region and oscillates at some point onward. This is because the energy of the carriers depends on the effective scattering time τ, and the charge carriers often move in a direction opposite to the direction of the applied magnetic field. Similar conclusions were reached in [16]. In contrast, the bandgap graphene has a smaller AME current, which can be tuned depending on the requirements of a particular device application and this highlights the novelty of our study. Both plots show virtually perfect oscillations superimposed as they monotonically tend to zero current. In the case where the spatial periodic structure of the SAW is present, this result might be interpreted as Weiss oscillations. Based on the commensurability between the electron cyclotron diameter at Fermi energy and the period of the electron modulation, this phenomenon is also observed to be periodic in the inverse magnetic field. The experimental setup shown in **Figure 1** [16] is suitable for verifying the phenomena for both components of the AME current density in the bandgap graphene as well. However, compared to gapless graphene, bandgap graphene is expected to perform far better because the bandgap can be tuned in a variety of ways, which will improve the electron population thereby making it suitable for use in electronic device applications.

Figure 4 shows a plot of the longitudinal (x-component) and Hall (y-component) of the AME current densities, $j_{x,y}^{AME}$ as functions of SAW frequency, ω_q for various values of the energy bandgap half-width Δ.

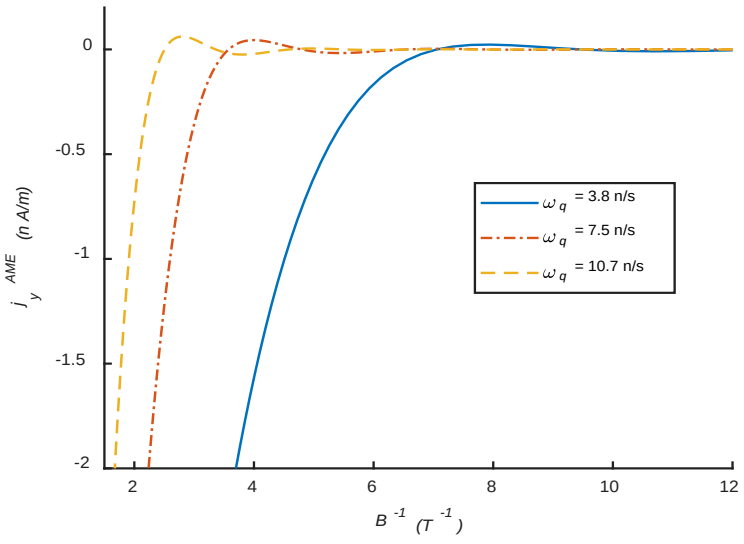

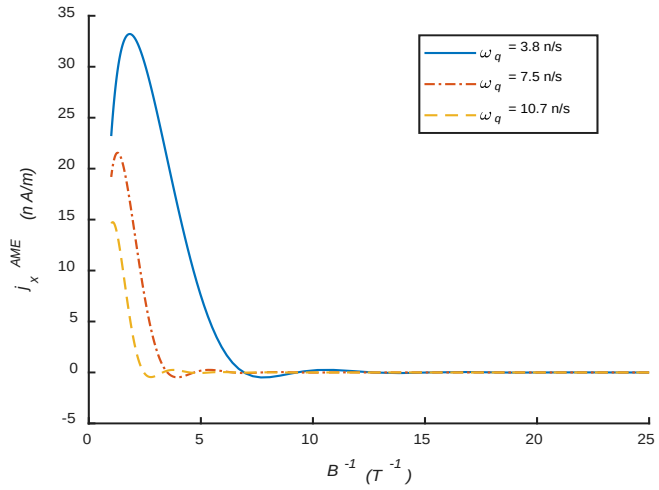

Figure 3. Acoustomagnetoelectric current density $\begin{pmatrix} j_x^{AME} \\ j_y^{AME} \end{pmatrix}$ as a function of inverse magnetic field B^{-1} at different SAW frequencies, ω_q.

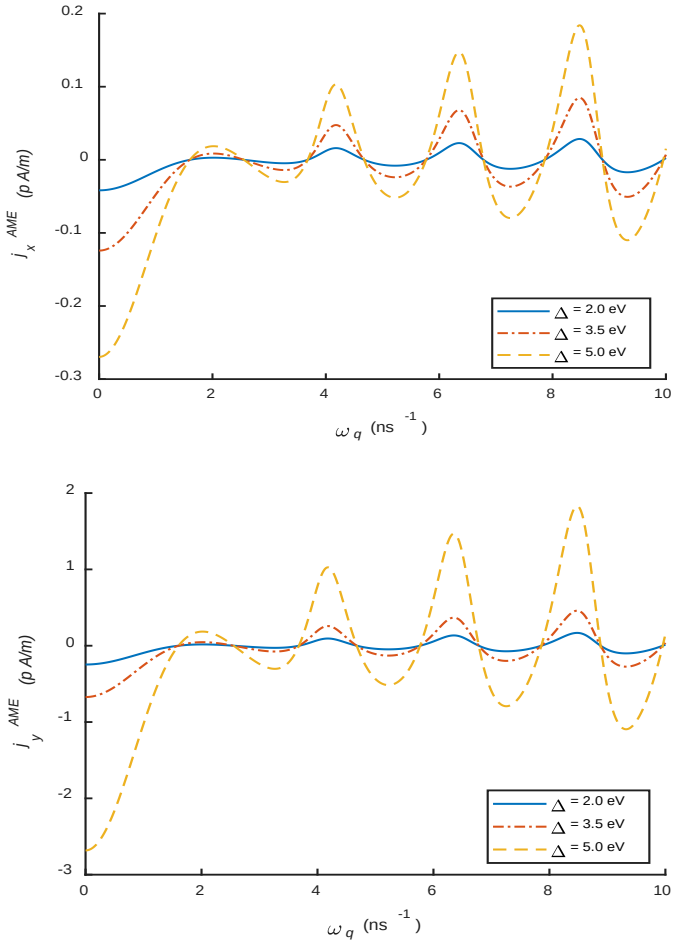

Figure 4. Acoustomagnetoelectric current density $\begin{pmatrix} j_x^{AME} \\ j_y^{AME} \end{pmatrix}$ as a function of SAW frequency ω_q forvarious energy bandgap half-width, Δ.

It can be inferred from Figure 4 that as ω_q increases, both components of the AME current density increase to a threshold value and oscillate about that point where both j_x^{AME} and j_y^{AME} equal zero. This results from the dependence of the energy on the bandgap half-width of the bandgap graphene. Additionally, the amplitudes of oscillations displayed in both graphs increase with increasing bandgap. Thus, increased bandgap half-width values lead to higher AME currents. As a result, the current density can be tuned using the bandgap half-width for device applications.

4. Conclusion

The AME current in graphene with an energy bandgap, where the energy is dependent on the bandgap created and the effective scattering time, has been studied using the semiclassical Boltzmann's transport equation. For a fixed magnetic field, the longitudinal and Hall components of the AME current density have been found to oscillate in response to the surface acoustic wave frequency. For a fixed surface acoustic wave frequency, the AME current oscillates in proportion to the inverse magnetic field, and the Hall component changes its sign in response to the Bessel function. The ratio of the surface acoustic wave and cyclotron frequencies or the ratio of the cyclotron radius and the surface acoustic wave wavelength can be used to represent the argument of the Bessel functions. The former occurs in Weiss oscillations of magnetoresistance when a static field is present, whereas the latter is usually used to describe optical geometric resonances. The study further demonstrated that the AME current density of the bandgap graphene, which can be tailored to a specific electronic device application, is smaller than that of gapless graphene and is, therefore, better suited for nanophotonic device applications.

Conflicts of Interest

The authors declare no conflicts of interest regarding the publication of this paper.

References

[1] Hernández-Mínguez, A., Liou, Y.T. and Santos, P.V. (2018) Interaction of Surface Acoustic Waves with Electronic Excitations in Graphene. *Journal of Physics D: Applied Physics*, **51**, Article 383001. https://doi.10.1088/1361-6463/aad593

[2] Aliofkhazraei, M., Ali, N., Milne, W.I., Ozkan, C.S., Mitura, S. and Gervasoni, J.L. (2016) Graphene Science Handbook: Electrical and Optical Properties. 1st Edition, CRC Press, Boca Raton. https://doi.org/10.1201/b19642

[3] Musah, R., Mensah, S.Y. and Abukari, S.S. (2014) Terahertz Generation and Amplification in Graphene Nanoribbons in Multi-Frequency Electric Fields. *Physica E: Low-dimensional Systems and Nanostructures*, **61**, 90-94. https://doi.org/10.1016/j.physe.2014.03.006

[4] Xia, F., Farmer, D.B., Lin, Y.M. and Avouris, P. (2010) Graphene Field-Effect Transistors with High on/off Current Ratio and Large Transport Band Gap at Room Temperature. *Nano Letters*, **10**, 715-718. https://doi.org/10.1021/nl9039636

[5] Meyer, J.C., Geim, A.K., Katsnelson, M.I., Novoselov, K.S., Booth, T.J. and Roth, S. (2007) The Structure of Suspended Graphene Sheets. *Nature*, **446**, 60-63. https://doi.org/10.1038/nature05545

[6] Poole, T. and Nash, G.R. (2017) Acoustoelectric Current in Graphene Nanoribbons. *Scientific Reports*, **7**, Article 1767. https://doi.org/10.1038/s41598-017-01979-8

[7] Gumbs, G., Aĭzin, G.R. and Pepper, M. (1999) Coulomb Interaction of Two Electrons in the Quantum Dot Formed by the Surface Acoustic Wave in a Narrow Channel. *Physical Review B*, **60**, Article R13954. https://doi.org/10.1103/PhysRevB.60.R13954

[8] Entin-Wohlman, O., Levinson, Y. and Galperin, Y.M. (2000) Acoustoelectric Effect in a Finite-Length Ballistic Quantum Channel. *Physical Review B*, **62**, Article 7283. https://doi.org/10.1103/PhysRevB.62.7283

[9] Mensah, S.Y., Allotey, F.K.A. and Adjepong, S.K. (1994) Acoustoelectric Effect in a Semiconductor Superlattice. *Journal of Physics*: *Condensed Matter*, **6**, Article 6783. https://doi.org/10.1088/0953-8984/6/34/010

[10] Lapa, P.N., Kassabian, G., Torres, F., Salev, P., Lee, M.H., Del Valle, J. and Schuller, I.K. (2020) Acoustoelectric Drag Current in Vanadium Oxide Films. *Journal of Applied Physics*, **128**, Article 155104. https://doi.org/10.1063/5.0015215

[11] Kalameitsev, A.V., Kovalev, V.M. and Savenko, I.G. (2019) Valley Acoustoelectric Effect. *Physical Review Letters*, **122**, Article 256801. https://doi.org/10.1103/PhysRevLett.122.256801

[12] Miseikis, V., Cunningham, J.E., Saeed, K., O'Rorke, R. and Davies, A.G. (2012) Acoustically Induced Current Flow in Graphene. *Applied Physics Letters*, **100**, Article 133105. https://doi.org/10.1063/1.3697403

[13] Sonowal, K., Kalameitsev, A.V., Kovalev, V.M. and Savenko, I.G. (2020) Acoustoelectric Effect in Two-Dimensional Dirac Materials Exposed to Rayleigh Surface Acoustic Waves. *Physical Review B*, **102**, Article 235405. https://doi.org/10.1103/PhysRevB.102.235405

[14] Fal'ko, V.I., Meshkov, S.V. and Iordanskii, S.V. (1993) Acoustoelectric Drag Effect in the Two-Dimensional Electron Gas at Strong Magnetic Field. *Physical Review B*, **47**, Article 9910. https://doi.org/10.1103/PhysRevB.47.9910

[15] Gurevich, V.L., Kozub, V.I. and Pevzner, V.B. (1998) Acoustoelectric Effect in Nanostructures: Role of Quasimomentum Balance. *Physical Review B*, **58**, Article 13088. https://doi.org/10.1103/PhysRevB.58.13088

[16] Savenko, I.G., Kalameitsev, A.V., Mourokh, L.G. and Kovalev, V.M. (2020) Acoustomagnetoelectric Effect in Two-Dimensional Materials: Geometric Resonances and Weiss Oscillations. *Physical Review B*, **102**, Article 045407. https://doi.org/10.1103/PhysRevB.102.045407

[17] Badicova, P.V. and Glazov, S.Y. (2015) Conductivity and Higher Current Density Harmonics of a Gap Graphene Modification in the Presence of Constant and Alternating Electric Fields. *Bulletin of the Russian Academy of Sciences*: *Physics*, **79**, 1443-1447. https://doi.org/10.3103/S1062873815120060

[18] Dompreh, K.A., Mensah, S.Y., Abukari, S.S., Edziah, R., Mensah, N.G. and Quaye, H.A. (2014) Acoustomagnetoelectric Effect in Graphene Nanoribbon in the Presence of External Electric and Magnetic Field. https://doi.org/10.48550/arXiv.1412.1678

[19] Zhao, P., Tiemann, L., Trieu, H.K. and Blick, R.H. (2020) Acoustically Driven Dirac Electrons in Monolayer Graphene. *Applied Physics Letters*, **116**, Article 103102. https://doi.org/10.1063/1.5139498